ACS APPLIED MATERIALS & INTERFACES

Research Article

www.acsami.org

Effects of TiO_2 Interfacial Atomic Layers on Device Performances and Exciton Dynamics in ZnO Nanorod Polymer Solar Cells

Mi-Jin Jin,[†] Junhyeon Jo,[†] Ji-Hee Kim,[‡] Ki-Seok An,[§] Mun Seok Jeong,[‡,⊥] Jeongyong Kim,*[,‡,⊥] and Jung-Woo Yoo*[,†]

[†]School of Materials Science and Engineering−Low Dimensional Carbon Materials Center, Ulsan National Institute of Science and Technology, Ulsan 688-798, Republic of Korea

[‡]IBS Center for Integrated Nanostructure Physics, Institute for Basic Science, Suwon 440-746, Republic of Korea

[⊥]Department of Energy Science, Sungkyunkwan University, Suwon 440-746, Republic of Korea

[§]Thin Film Materials Research Group, Korea Research Institute of Chemical Technology, Daejeon 305-543, Republic of Korea

Supporting Information

ABSTRACT: The performances of organic electronic and/or photonic devices rely heavily on the nature of the inorganic/organic interface. Control over such hybrid interface properties has been an important issue for optimizing the performances of polymer solar cells bearing metal-oxide conducting channels. In this work, we studied the effects of an interfacial atomic layer in an inverted polymer solar cell based on a ZnO nanorod array on the device performance as well as the dynamics of the photoexcited carriers. We adopted highly conformal TiO_2 interfacial layer using plasma enhanced atomic layer deposition (PEALD) to improve the compatibility between the solution-prepared active layer and the ZnO nanorod array. The TiO_2 interfacial layer facilitated exciton separation and subsequent charge transfer into the nanorod channel, and it suppressed recombination of photogenerated carriers at the interface. The presence of even 1 PEALD cycle of TiO_2 coating substantially improved the short-circuit current density (J_{sc}), open circuit voltage (V_{oc}), and fill factor (FF), leading to more than 2-fold enhancement in the power conversion efficiency (PCE). The dynamics of the photoexcited carriers in our devices were studied using transient absorption (TA) spectroscopy. The TA results clearly revealed that the TiO_2 coating played a key role as an efficient quencher of photogenerated excitons, thereby reducing the exciton lifetime. The electrochemical impedance spectra (EIS) provided further evidence that the TiO_2 atomic interfacial layer promoted the charge transfer at the interface by suppressing recombination loss.

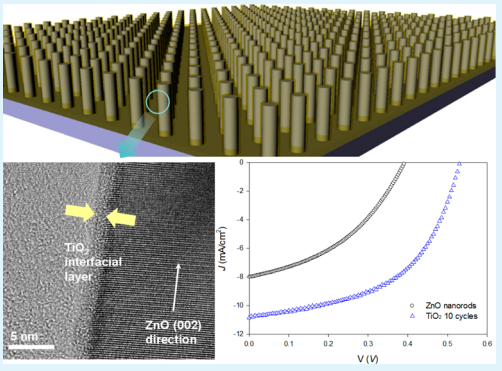

KEYWORDS: *solar cell, hybrid interface, ZnO nanorod, atomic layer deposition, transient absorption, electrochemical impedance spectroscopy*

1. INTRODUCTION

Polymer solar cells have been considered as one of the most important alternatives to conventional power generation, because they are lightweight, flexible, low-cost, and suitable for large area cell production. Developing appropriate materials and device structures has been a key factor to facilitating improved device performance of polymer solar cells.[1] To overcome limited exciton diffusion length in polymer, the concept of bulk heterojunction (BHJ) based on a self-assembled phase separation of a conjugated polymer and a fullerene derivative has been widely adopted in polymer solar cells.[2,3] This BHJ creates a large interfacial area between electron donor and acceptor and provides shorter distance for the photoexcited excitons to the interfaces leading to efficient exciton separation. However, disordered charge transport pathways due to randomly separated nanosize phases in the bulk are not desirable for the collection of photocurrent.[4,5] Significant progresses toward increasing power conversion efficiencies (PCEs) have been achieved by assembling inorganic nanostructured acceptors that provide electron conducting channels with higher mobilities.[6] A variety of inorganic nanomaterials, including TiO_2,[7−9] ZnO,[10−14] PbS,[15] PbSe,[16] CdS,[17] CdSe,[18] CdTe,[19] have been used as acceptors in hybrid polymer solar cells. But the disordered assembly of nanomaterials also limits the flow of photocurrent and introduces charge traps in the bulk, leading to recombination loss. Moreover, percolation networks are sensitive to the experimental processes associated with materials and device fabrications, making it difficult to achieve a reliable device performance.

Vertically aligned nanostructures have been implemented in polymer solar cells in an effort to overcome the above problems

Received: April 22, 2014
Accepted: July 2, 2014
Published: July 2, 2014

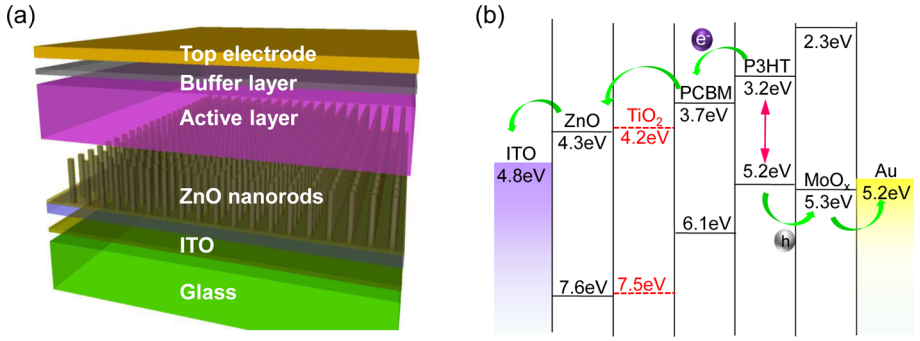

Figure 1. (a) Device structure of the hybrid polymer solar cell prepared with a TiO_2-coated ZnO nanorod electron conductive channel. (b) Schematic view of the energy band diagram of the studied hybrid polymer solar cell.

by providing robust charge transport pathways to the electrode.[20−28] ZnO nanorod arrays have been extensively investigated for their use as electron conducting channels in hybrid polymer solar cells.[23−29] ZnO is a wide band gap semiconductor with an energy gap of 3.3 eV and a conduction band edge of 4.3 eV. This band edge is sufficiently high to extract electrons from typical donor and acceptor molecules and/or polymers. The relatively high electron mobility of the material makes it suitable as an electron transport layer in hybrid polymer solar cells. But the ZnO nanorod polymer solar cells have not yet lived up to expectations because of the poor interface properties.[23−29] Poor interface properties can arise from a low infiltration of the polymer into the deep valleys of the nanostructure.[1,30] Morphology effects can introduce trapped charges into the separated phases.[31] The as-grown ZnO nanorods generally contain large amounts of surface defects, and the ZnO/organic interfaces can also introduce charge transfer and unwanted dipoles.[32−34] The potential pinning due to poorly controlled interface dipoles can significantly affect the built-in potential in the bulk, thereby suppressing the open circuit voltage (V_{oc}) of a device.[35] Recombination loss due to trapped charges from such surface defects and interface dipoles breaks the balance between charge creation and extraction and significantly reduces the performances of hybrid solar cells. Therefore, the reduced device performance of hybrid nanostructure cell is rather due to the charge extraction limits than the charge generation. Controlling the interfacial properties and their influences on charge extraction has been central to the design of efficient hybrid polymer solar cells.[36−41]

One of the main approaches to modifying oxide nanostructure surfaces has involved using a variety of organic dyes and small molecules[42−50] to improve the affinity between the ZnO surface and the organic BHJ. These interfacial organic species can improve exciton dissociation at the hybrid interface and reduce the recombination rate. In addition, they can absorb incident light and actively harvest the photocurrent.[51]

Though organic dyes and small molecules can enhance the compatibility between oxide and organic interfaces, passivation of surface defects and the chemical reactivity of the as-grown ZnO nanorods could be achieved more effectively by introducing a wide band gap oxide film coating onto the ZnO nanorods.[52−54] ZnO-TiO_2 core−shell nanostructures, which exploit both the high stability of TiO_2 and the high electron mobility of ZnO, present a promising solution to the charge collection issue in hybrid polymer solar cells. Several studies reported enhanced device performance upon the introduction of a TiO_2 coating onto the ZnO nanorods in a hybrid polymer solar cell with a P3HT active layer.[55−59] But, the performances of the devices studied were not as satisfactory as those of the BHJ solar cells. And the TiO_2 capping layers in those studies typically exceeded 10 nm in thickness, implying that the TiO_2 layer functioned as an additional conducting layer rather than an interface modifier.

In this work, we studied the effects of TiO_2 interfacial atomic layers on the performances of ZnO nanorod polymer solar cells and the corresponding exciton dynamics. A BHJ of P3HT (poly-3-hexylthiophene):PCBM (Phenyl-C71-butyric acid methyl ester) was used for the active layer. The ZnO/BHJ interfaces were modified by highly conformal TiO_2 atomic layer developed by plasma enhanced atomic layer deposition (PEALD). Variation of 1 to 10 cycles of TiO_2 coatings was employed to study the effects of interface modifications on photovoltaic device performances. In addition to the device characterization, we employed transient absorption (TA) measurements to study the effective lifetimes of the photogenerated excitons and their quenching. A TiO_2 interfacial layer introduced substantial improvement in the performance of hybrid polymer solar cell. The device characteristics, such as the V_{oc}, short-circuit current density (J_{sc}), fill factor (FF), and ideality factor (n), improved significantly upon the introduction of even 1 cycle of TiO_2 coating. The transient absorption (TA) spectra indicated that the ultrathin TiO_2 interfacial layer functioned as an efficient quencher by suppressing the lifetime of the photogenerated excitons. Moreover, electrochemical impedance spectroscopy (EIS) clearly showed reduced recombination rate at the interface by the TiO_2 coating.

2. EXPERIMENTAL SECTION

2.1. Device Structure. Panels a and b in Figure 1 display the device structure of the bulk heterojunction solar cell studied here and a schematic diagram showing the photovoltaic process in our devices, respectively. In this device configuration, which is sort of inverted-type, the photogenerated electrons and holes are collected through opposite pathway to that in the conventional BHJ solar cell, i.e., the generated electrons are collected at the ITO cathode, whereas the generated holes are collected at the top Au electrode. The ZnO nanorods, which functioned as an electron-conducting channel, were coated with a ultrathin TiO_2 film to facilitate charge separation and suppress interfacial recombination.

2.2. Preparation of ZnO nanorods and TiO_2 Interfacial Atomic Layer. The ZnO nanorod templates were prepared on top of ITO/glass substrates using the sol−gel method. The sol−gel solution, which was prepared with zinc acetate with methoxy ethanol and ethanol amine, was spin-coated on the substrate (~40 nm thickness) followed by 30 min annealing at 300 °C.[60] The film was then kept 30 min in a 90 °C of D.I water with 0.01 M of zinc nitrate ($Zn(NO)_3 \cdot 6H_2O$) as a cation and 0.01 M of hexadimethylenetetramine (HMT,

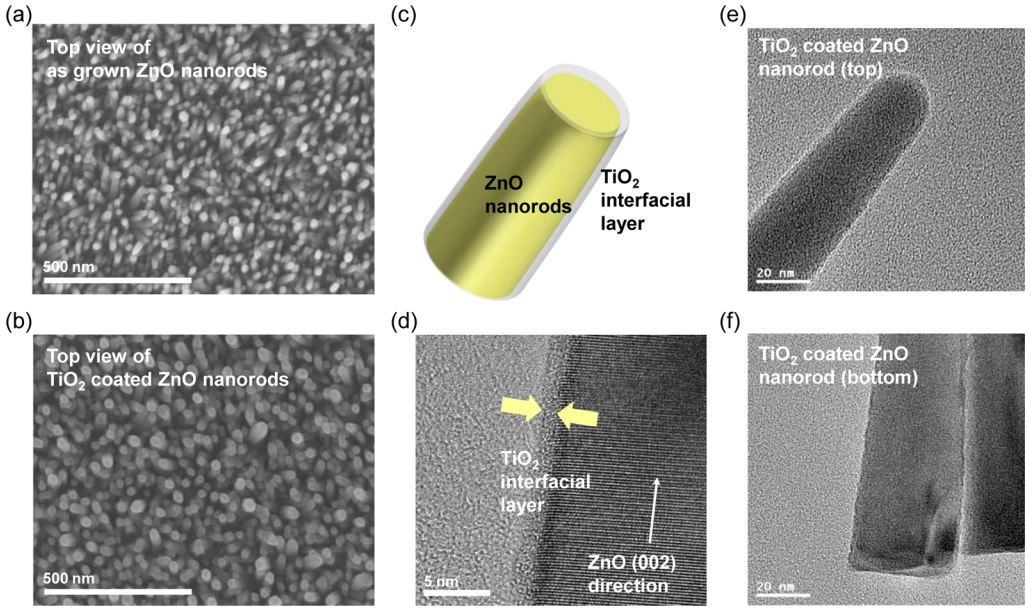

Figure 2. (a) Top-view FE-SEM image of the as-grown ZnO nanorod template. (b) Top-view FE-SEM image of TiO_2-coated ZnO nanorod template (TiO_2 coating of 10 PEALD cycles). The magnification used for the SEM images was 50,000. (c) Schematic view of the conformal TiO_2 coating on the ZnO nanorods. (d) HR-TEM image of TiO_2-coated ZnO nanorods. The TiO_2 coating was performed for 10 PEALD cycles to produce a 1.6 nm thick film. The image also displayed the (100) directional growth of the ZnO nanorods. (e, f) HR-TEM images of the top and bottom parts of TiO_2-coated ZnO nanorods. The HR-TEM images showed conformal growth of the TiO_2 layer over the top to the bottom of the ZnO nanorods.

$(CH_2)_6N_4$) as a hydroxide anion precursors. Typical heights of the ZnO nanorods were 300 nm.

On the surfaces of the ZnO nanorod arrays, highly conformal TiO_2 layers were coated by using the PEALD method. Sequential injections of TDMAT (tetrakis-dimethyl-amino-titanium) and a mixture of Ar and O_2 plasma were used to form a TiO_2 layer with a growth temperature of 200 °C. The TDMAT purchased from STREM was used for the PEALD process. The Ar gas and O_2 gas flow rates for generating the Ar-assisted oxygen plasma were 10 and 1 sccm, respectively. A 180 W RF (radio frequency, 13.56 MHz) power source was applied to generate the oxygen plasma. For one cycle of TiO_2 film growth, TDMAT precursor was first injected into the growth chamber for 0.08 s. Then, the chamber was purged with Ar gas for 50 s to remove residues and other impurities. The Ar-assisted oxygen plasma was then ignited and maintained for 20 s. Finally, the chamber was purged with the Ar gas (10 sccm) to remove any remaining residues. TiO_2 coatings of 1 to 10 cycles on the ZnO nanorod arrays were employed to study the effects of the modified oxide/organic interfaces. The growth rate of the PEALD TiO_2 film was estimated to be 1.6 Å/cycle.

2.3. Device Fabrication and Characterization. A P3HT (poly(3-hexylthiophene), regioregularity 98%): PCBM (Phenyl-C71-butyric acid methyl ester) blend with a 1:1 mass ratio was used for the active layer of the hybrid polymer solar cell. Both P3HT and PCBM were purchased from Aldrich and used without further purification. The blend was dissolved in chlorobenzene (99.8%) and applied by spin-coating at 700 rpm for 120 s. The spin-coated film was then annealed at 150 °C for 10 min. The typical thickness of the active layer was estimated to be 400 nm. Finally, MoO_x(5 nm)/Au(60 nm) layers were thermally deposited in sequence to create the hole conducting layer. The photovoltaic properties were tested by using a solar simulator (Abet technology, xenon lamp) and $J-V$ measurement system (IVIUM technologies) upon A.M 1.5 mass illumination (100 mW/cm^2). EIS was performed by using VersaSTAT3 from Princeton Applied Research. The measured frequency range was 0.1 to 1×10^6 Hz. The magnitude of the alternating voltage was 10 mV. The measurements were done under the dark condition without DC bias.

2.4. TA Spectroscopic Measurement. TA mappings were measured at room temperature by employing a Helios-Femtosecond TA spectrometer (Ultrafast systems, Helios) with a pump pulse of 350 nm center wavelength (Light conversion, TOPAS prime) and a white-light-continuum in the visible region as a probe pulse, derived from a Ti:sapphire amplifier (Coherent, Libra series). The temporal resolution was around 200 fs, depending on the pulse duration of the pump. Here, we display both the TA spectra at different time delays and the kinetics of the TA obtained at a probe wavelength of 640 nm, the P3HT absorption band, to observe the charge separation phenomena at the interface between the ZnO nanorods and the P3HT/PCBM.

3. RESULTS AND DISCUSSION

Images a and b in Figure 2 show top view field-emission scanning electron microscopy (FE-SEM) images of the as-grown ZnO nanorods and TiO_2-coated ZnO nanorods prepared using 10 cycles of PEALD. The thickness of TiO_2 layer for 10 PEALD cycles was estimated to be 1.6 nm. The magnification used for the SEM images was 50,000. A uniform TiO_2 coating on the ZnO nanorod surface can be clearly observed in high resolution transmission electron microscopy (HR-TEM) images (Figure 2d–f). Figure 2d shows the amorphous growth of the TiO_2 layer and the crystalinity of the ZnO nanorod. The X-ray diffraction pattern showed (002) directional growth of ZnO nanorods indicating the hexagonal wurtzite phase of ZnO (see Figure S1 in the Supporting Information). No diffraction pattern was observed for TiO_2 capping layer. Images e and f in Figure 2 show HR-TEM images of the top and bottom parts of the nanorod and clearly demonstrate a conformal growth of the TiO_2 layer on ZnO nanorods. UV–vis transmission spectra displayed that the changes in light absorption by ultrathin TiO_2 coatings were not significant (see Figure S2 in the Supporting Information).

Figure 3 displays the characteristic current density–voltage ($J-V$) curves for a series of cell devices prepared with or without a TiO_2 coating on the ZnO nanorods. The TiO_2 coatings were done for 1, 3, 5, 7, or 10 PEALD cycles,

dx.doi.org/10.1021/am5024435 | ACS Appl. Mater. Interfaces 2014, 6, 11649–11656

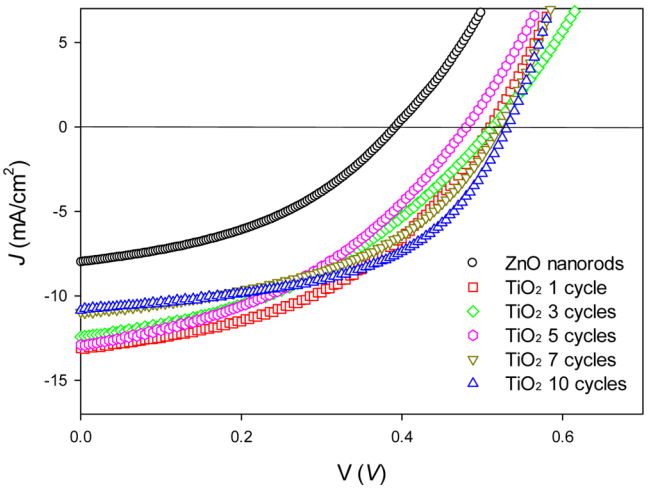

Figure 3. Characteristic $J-V$ curves for the studied cell devices prepared with or without a TiO_2 coating on the ZnO electron channels. TiO_2 coatings were applied over 1, 3, 5, 7, or 10 PEALD cycles.

respectively. Significant improvements in the characteristic parameters, such as V_{oc}, J_{sc}, and FF, were clearly observed upon introduction of the TiO_2 interfacial layer. Surprisingly, even 1 cycle of TiO_2 coating introduced substantial improvements in the overall device performance. The broadband external quantum efficiencies (EQEs) were also tested for the series of cell devices with or without a TiO_2 coating. TiO_2 coatings introduced significant enhancement of EQE over the wavelength range of 370−650 nm (see Figure S3 in the Supporting Information). Note that this enhancement of EQE is not correlated with the change in absorption by the TiO_2 coating. The dependence of device performance on the thickness of TiO_2 film did not display general trend. However, capping of the TiO_2 layer over 15 PEALD cycles induces decreased V_{oc}, J_{sc}, and FF, leading to significant reductions in cell performances (see Figure S4 in the Supporting Information). While the TiO_2 interfacial layer could function as a charge-separating and/or a defect-tolerating layer, increasing thickness of the TiO_2 layer introduces an additional conducting channel with higher resistance, which is not desirable for the efficient charge collection. The characteristic parameters of the $J-V$ curves for a series of solar cells are summarized in Table 1. Each value in Table 1 was obtained from more than 8 sample devices.

The device performances of the ZnO nanorod solar cells prepared without a TiO_2 interfacial layer were poor, with averaged PCE of less than 1%. This unsatisfactory device performances arose from the poor interface quality between the ZnO and the active layer, which generated recombination loss due to trapped charges,[31−34] and midgap behavior of ZnO, which could alter the interfacial energetic differences in the bulk.[35] It should be also noted that the best results for the inverted polymer solar cell with the P3HT:PCBM active layer and the ZnO electron conductive layer displayed PCEs as high as ∼3−5%.[61−64] The reduction of PCE in our device can be partly attributed to the increased thickness of the active layer due to the inclusion of ZnO nanorods. The addition of a TiO_2 layer to our cell devices significantly enhanced both V_{oc} and J_{sc} compared to the values obtained from devices prepared with bare ZnO nanorods. Moreover, the *PCEs* were improved by more than 2-fold (see Table 1). The significant performance improvements were attributed to the fact that the TiO_2 layer facilitated charge extraction by assisting effective exciton dissociation and recombination quenching. As displayed in Figure 1b, the electronic structures of ZnO and TiO_2 were very similar. But the concentration gradient in ZnO-TiO_2 core−shell structure can induce a built-in potential ($\Delta\phi$), as follows[65−68]

$$\Delta\varphi = \frac{kT}{q}\ln\frac{N_e^+}{N_e} \quad (1)$$

where k is Boltzmann's constant, q is the electron charge, N_e^+ and N_e are the electron concentration in the ZnO core and the TiO_2 shell, respectively. This built-in potential drives electron carriers to drift against the concentration gradient and eventually confines them into the ZnO core. Therefore, recombination loss at the ZnO-TiO_2 core−shell/BHJ interface can be substantially reduced, although the intrinsic band structure of TiO_2 did not provide an energetic barrier. In addition, the physical separation enabled by the TiO_2 layer may alleviate ZnO midgap behavior[35] at the interface and maintain V_{oc}.

Figure 4 shows the dark $J-V$ characteristics for the studied solar cells. The transition from exponential behavior to the space-charge limited regime reflects the built-in voltage, which is often derived from the energetic difference between the LUMO of the electron acceptor and the HOMO of the hole transporting active layer. The current density at a low bias can be considered as a leakage contribution. As shown in Figure 4, the device prepared with a bare ZnO nanorod array showed a large leak current. The addition of a TiO_2 layer on the ZnO nanorods effectively reduced the leak current and maintained the built-in voltage. The inset of Figure 4 displays the ideality factors of the studied cell devices, determined from the semilogarithmic $J-V$ plots, as shown

$$n = \left(\frac{kT}{q}\frac{\partial \ln J}{\partial V}\right)^{-1} \quad (2)$$

For an ideal p−n junction diode, in which charge carrier traps and recombination are negligible, the ideality factor should be close to the unity. The ideality factors greater than unity were

Table 1. Characteristic Parameters of the $J-V$ Curves Obtained from the Studied Cell Devices[a]

	V_{oc} (V)	I_{sc} (mA)	J_{sc} (mA/cm²)	FF	PCE (%)
ZnO NRs	0.35 ± 0.01	0.73 ± 0.03	6.09 ± 0.26	0.40 ± 0.03	0.89 ± 0.17
TiO_2-coated ZnO NRs (1 cycle) (1 cycle)	0.52 ± 0.01	1.51 ± 0.05	12.51 ± 0.62	0.38 ± 0.03	2.45 ± 0.28
TiO_2-coated ZnO NRs (3 cycles) (3 cycles)	0.54 ± 0.02	1.41 ± 0.04	11.75 ± 0.40	0.37 ± 0.02	2.30 ± 0.11
TiO_2-coated ZnO NRs (5 cycles) (5 cycles)	0.46 ± 0.02	1.58 ± 0.05	13.17 ± 0.56	0.38 ± 0.03	2.29 ± 0.27
TiO_2-coated ZnO NRs (7 cycles) (7 cycles)	0.54 ± 0.01	1.23 ± 0.02	10.29 ± 0.21	0.57 ± 0.03	3.15 ± 0.06
TiO_2-coated ZnO NRs (10 cycles) (10 cycles)	0.54 ± 0.01	1.33 ± 0.03	11.06 ± 0.28	0.55 ± 0.06	3.26 ± 0.35

[a]Each value was obtained from more than 8 sample devices.

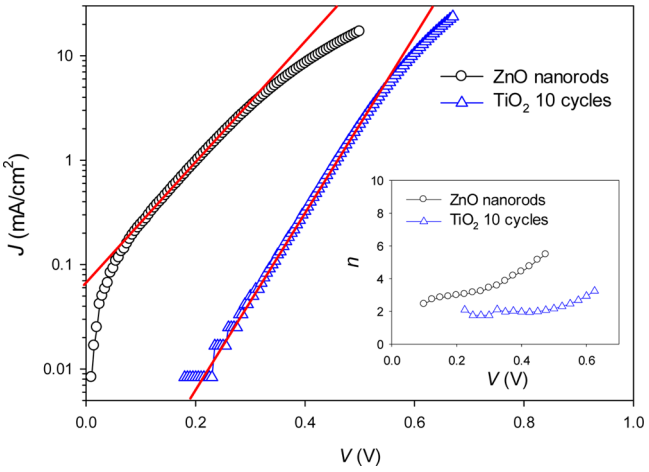

Figure 4. Semilogarithmic dark $J-V$ characteristic curves for the cell devices prepared with ZnO nanorods or TiO_2-coated ZnO nanorods. The inset shows a plot of the ideality factor (n) according to eq 2

attributed to the trap-assisted recombination in the space-charge region.[69−72] Our cell devices based on bare ZnO nanorods exhibited poor diode curve and high ideality factor values. Such device characteristics arose mainly from recombination loss due to the charge traps at the separated phases in nanostructures and at the oxide/organic interfaces. Devices with TiO_2 coatings showed significant improvements in diode ideality factors. The TiO_2 interfacial atomic layer played an important role in reducing charge traps and recombination. Thus, it can assist balancing between charge generation and extraction, and finally lead to the significant improvement in the overall device performance.

TA is a powerful tool for observing transient charge carriers, generated by photoexcitation, either in radiative or nonradiative processes. TA has been utilized to study the time-resolved phenomena involved in the photovoltaic conversion processes in solar cells.[73−75] On the basis of TA results, generation and recombination mechanisms of transient charge carriers and their dynamics in the polymer solar cells can be effectively described.[73−76]

Exciton charge separation at the interfaces within our nanostructure solar cells was investigated by performing TA spectroscopy on two different samples, ZnO nanorods-only (ZnO-only), and ZnO nanorods prepared with a TiO_2 coating of 5 PEALD cycles (5-cycle). Panels a and b in Figure 5 show the TA spectra at different time delays, obtained from two samples. The TA signal is, in general, interpreted as a combination of excitonic photobleaching (PB) and photo-induced absorption (PA) processes. Here, the negative band below 620 nm corresponded to the ground-state absorption of the device or, alternatively, to the PB. The TA signal above 630 nm turned into positive values due to PA by the excitons in the blend. From the difference between shorter (5 ps) and longer (300 ps) time delay at 640 nm, we notice that variation appeared in the sample with TiO_2 coating is over 25% larger than that of the pristine ZnO sample. This result suggested that the photogenerated charges were well-separated in the blend and were efficiently transferred through the TiO_2 layers. Note that the time-resolved responses in the 510 and 590 nm PB band were indistinguishable. The decay times in the ZnO-only and the 5-cycle samples were characterized by fitting the TA kinetics to a multiexponential function at the probe wavelength of 640 nm (see Figure 5c). The fast decay components (<10 ps) corresponded to nonradiative recombination channels, whereas the slow decay components corresponded to charge transfer processes. The charge transfer time constants were 150 ps for the 5-cycle and 164 ps for the ZnO-only samples. These results supported our interpretation of the role of the TiO_2 layer in the device operation. As the TiO_2 layer was inserted between the BHJ and ZnO nanorods, the slow decay time constant decreased because the layer acted as a new relaxation channel and enhanced charge separation.[21]

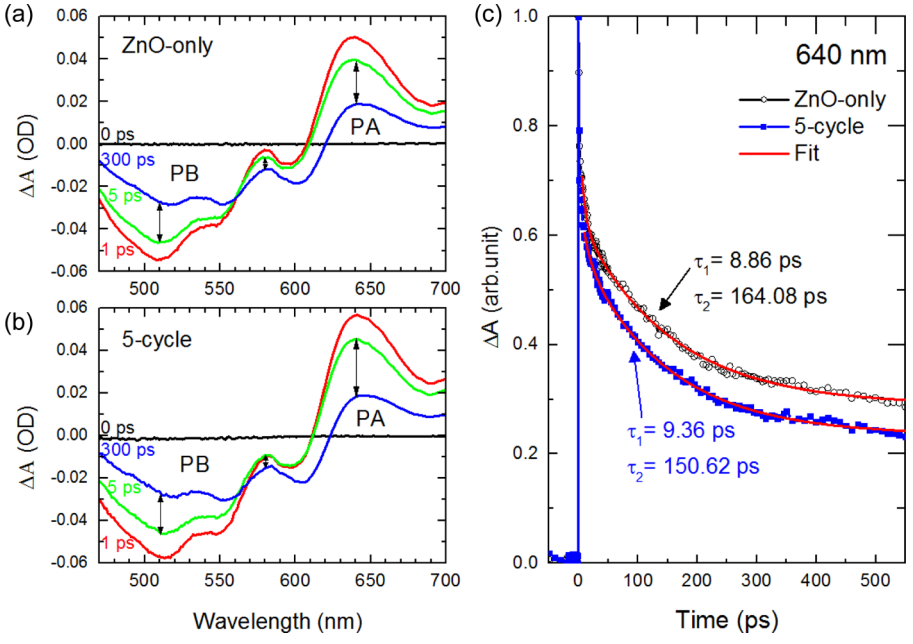

Figure 5. TA spectra collected at different time delays in (a) the ZnO nanorod-only, and (b) 5-cycle TiO_2 coating devices. (c) TA kinetics at a probe wavelength of 640 nm, obtained from the ZnO-only (open circle), and from the 5-cycle (filled square) devices, respectively. The red curves represent the exponential fits to the data.

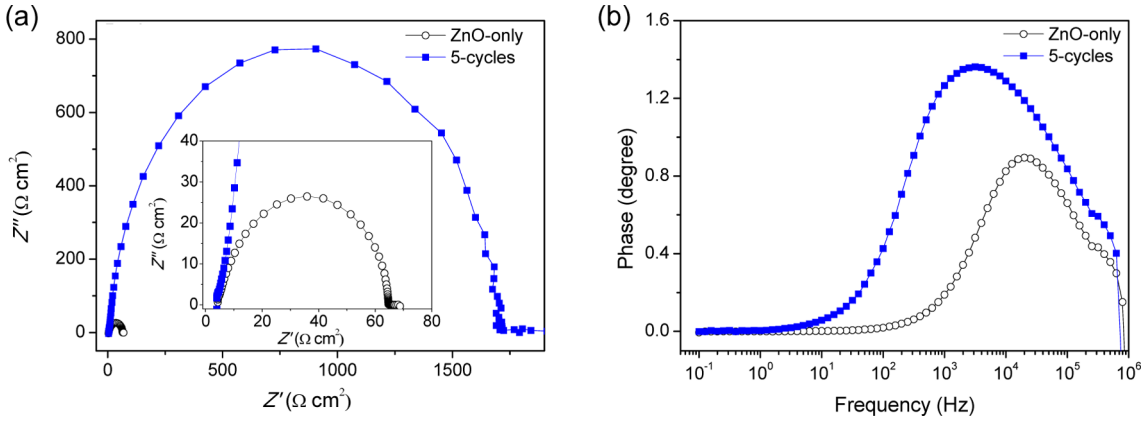

Figure 6. EIS spectra of cell devices with ZnO nanorod-only (open circle) and 5-cycle TiO_2 coating (filled square) (a) Nyquist plots in complex impedance plane. (b) Bode phase angle versus frequency plots.

The role of the TiO_2 capping layer in our cell device can be more clearly observed in EIS, which directly probes the charge transfer passing through the ZnO-TiO_2 core−shell/BHJ interface. EIS measurements were also performed for two different sample devices, one with ZnO nanorods-only (ZnO-only) and the other with ZnO nanorods coated with TiO_2 layer of 5 PEALD cycles (5-cycle). Figure 6a displays Nyquist plots of EIS spectra, which was measured for cell devices of ZnO-only and 5-cycle under the dark condition without DC bias. EIS spectra display semicircles in complex plane for both samples with significant difference in the magnitude of the impedance. The peak frequencies of semicircles are 19952 Hz for ZnO-only and 3162 Hz for 5-cycle, respectively. The impedance in medium frequency of 10 to 1×10^5 Hz is associated with the charge transfer at the interfaces.[77] In general, the larger the size of the semicircle is, the stronger is the recombination resistance at the interface.[77−80] The semicircle representing cell device with 5-cycle is significantly larger than that of cell device with ZnO-only. The enhanced recombination resistance suggests longer electron lifetimes, which can be deduced from the relation $\tau_e = (2\pi f_{max})^{-1}$. The longer electron recombination lifetime due to the TiO_2 coating is directly noticeable in Bode phase plots of Figure 6b, which displays strong left-shift of the characteristic frequency by 1 order of magnitude. This significant reduction of the recombination rate at the interfaces due to TiO_2 coating leads to the improved J_{sc}, V_{oc}, FF, and PCE of the studied hybrid polymer solar cell.

4. CONCLUSIONS

In conclusion, we studied the effects of modifying the oxide/organic interfaces in hybrid polymer solar cells on device performance. Insertion of TiO_2 interfacial atomic layer at ZnO/organic interface by PEALD significantly improved cell characteristics, such as V_{oc}, J_{sc}, FF, and PCE. These improvements were attributed to the enhanced charge extraction by the TiO_2 interfacial layer. Both TA and EIS spectra indicate that the TiO_2 interfacial layer functions as an efficient photogenerated exciton quencher and assisted effective charge collection.

■ ASSOCIATED CONTENT

Supporting Information

XRD pattern of ZnO nanorod on ITO substrate. UV−vis transmission spectra for ZnO nanorods and ZnO nanorods with TiO_2 coatings of 1, 5, 7, and 10 PEALD cycles. EQE spectra for cell devices with ZnO nanorods and ZnO nanorods with TiO_2 coatings of 1, 5, 7, and 10 PEALD cycles. $J-V$ characteristics of cell devices with TiO_2 coatings of 15, 20, 30 PEALD cycles. This material is available free of charge via the Internet at http://pubs.acs.org.

■ AUTHOR INFORMATION

Corresponding Authors

*E-mail: j.kim@skku.edu.
*E-mail: jwyoo@unist.ac.kr.

Notes

The authors declare no competing financial interest.

■ ACKNOWLEDGMENTS

This work was supported by the National Research Foundation of Korea (NRF) grant (2011-0014651) funded by the Ministry of Education, Science and Technology. This research was also supported by a grant from (Future Challenge Project or Creativity and Innovation Project) funded by the UNIST (Ulsan National Institute of Science and Technology). Ki-Seok An was supported by a grant (2011-0031636) from the Center for Advanced Soft Electronics under the Global Frontier Research Program of the Ministry of Science, ICT and Future Planning, Korea.

■ REFERENCES

(1) Brabec, C.; Dyakonov, V.; Scherf, U. *Organic Photovoltaics: Materials, Device Physics, and Manufacturing Technologies*; Wiley-VCH: Weinheim, Germany, 2008.
(2) Yu, G.; Gao, J.; Hummelen, J. C.; Wudl, F.; Heeger, A. J. Polymer Photovoltaic Cells: Enhanced Efficiencies via a Network of Internal Donor-acceptor Heterojunctions. *Science* **1995**, *270*, 1789−1791.
(3) Halls, J. J. M.; Walsh, C. A.; Greenham, N. C.; Marseglia, E. A.; Friend, R. H.; Moratti, S. C.; Holmes, A. B. Efficient Photodiodes from Interpenetrating Polymer Networks. *Nature* **1995**, *376*, 498−500.
(4) Schilinsky, P.; Waldauf, C.; Brabec, C. J. Recombination and Loss Analysis in Polythiophene Based Bulk Heterojunction Photodetectors. *Appl. Phys. Lett.* **2002**, *81*, 3885−3887.
(5) Huynh, W. U.; Dittmer, J. J.; Teclemariam, N.; Milliron, D. J.; Alivisatos, A. P.; Barnham, K. W. J. Charge Transport in Hybrid Nanorod-Polymer Composite Photovoltaic Cells. *Phys. Rev. B* **2003**, *67*, 125326.
(6) Bouclé, J.; Ackermann, J. Solid-state Dye-Sensitized and Bulk Heterojunction Solar Cells Using TiO_2 and ZnO Nanostructures: Recent Progress and New Concepts at the Borderline. *Polym. Int.* **2012**, *61*, 355−373.
(7) Kwong, C. Y.; Djurisic, A. B.; Chui, P. C.; Cheng, K. W.; Chan, K. W. Influence of Solvent on Film Morphology and Device Performance

of Poly(3-hexylthiophene): TiO_2 Nanocomposite Solar Cells. *Chem. Phys. Lett.* **2004**, *384*, 372−375.
(8) van Hal, P. A.; Wienk, M. M.; Kroon, J. M.; Verhees, W. J. H.; Slooff, L. H.; van Gennip, W. J. H.; Jonkheijm, P.; Janssen, R. A. J. Photoinduced Electron Transfer and Photovoltaic Response of a MDMO-PPV: TiO_2 Bulk-Heterojunction. *Adv. Mater.* **2003**, *15*, 118−121.
(9) Wang, M.; Wang, X. P3HT/TiO_2 Bulk-Heterojunction Solar Sell Sensitized by a Perylene Derivative. *Sol. Energy Mater. Sol. Cells* **2007**, *91*, 1782−1787.
(10) Beek, W. J. E.; Wienk, M. M.; Janssen, R. A. J. Efficient Hybrid Solar Cells from Zinc Oxide Nanoparticles and a Conjugated Polymer. *Adv. Mater.* **2004**, *16*, 1009−1013.
(11) Beek, W. J. E.; Slooff, L. H.; Wienk, M. M.; Kroon, J. M.; Janssen, R. A. J. Hybrid Solar Cells Using a Zinc Oxide Precursor and a Conjugated Polymer. *Adv. Funct. Mater.* **2005**, *15*, 1703−1707.
(12) Beek, W. J. E.; Wienk, M. M.; Kemerink, M.; Yang, X.; Janssen, R. A. J. Hybrid Zinc Oxide Conjugated Polymer Bulk Heterojunction Solar Cells. *J. Phys. Chem. B* **2005**, *109*, 9505−9516.
(13) Hau, S. K.; Yip, H.-L.; Baek, N. S.; Zou, J.; O'Malley, K.; Jen, A. K. Y. Air-Stable Inverted Flexible Polymer Solar Cells Using Zinc Oxide Nanoparticles as an Electron Selective Layer. *Appl. Phys. Lett.* **2008**, *92*, 253301.
(14) Wang, M.; Wang, X. P3HT/ZnO Bulk-Heterojunction Solar Cell Sensitized by a Perylene Derivative. *Sol. Energy Mater. Sol. Cells* **2008**, *92*, 766−771.
(15) Fritz, K. P.; Guenes, S.; Luther, J.; Kumar, S.; Sariciftci, N. S.; Scholes, G. D. IV−VI Nanocrystal−Polymer Solar Cells. *J. Photochem. Photobiol., A* **2008**, *195*, 39−46.
(16) Qi, D.; Fischbein, M.; Drndić, M.; Šelmić, S. Efficient Polymer-Nanocrystal Quantum-Dot Photodetectors. *Appl. Phys. Lett.* **2005**, *86*, 093103.
(17) Ren, S.; Chang, L.-Y.; Lim, S.-K.; Zhao, J.; Smith, M.; Zhao, N.; Bulović, V.; Bawendi, M.; Gradečak, S. Inorganic−Organic Hybrid Solar Cell: Bridging Quantum Dots to Conjugated Polymer Nanowires. *Nano Lett.* **2011**, *11*, 3998−4002.
(18) Huynh, W. U.; Dittmer, J. J.; Alivisatos, A. P. Hybrid Nanorod-Polymer Solar Cells. *Science* **2002**, *295*, 2425−2427.
(19) Chen, Z.; Zhang, H.; Du, X.; Cheng, X.; Chen, X.; Jiang, Y.; Yang, B. From Planar-Heterojunction to n−i Structure: an Efficient Strategy to Improve Short-Circuit Current and Power Conversion Efficiency of Aqueous-Solution-Processed Hybrid Solar Cells. *Energy Environ. Sci.* **2013**, *6*, 1597−1603.
(20) Mor, G. K.; Shankar, K.; Paulose, M.; Varghese, O. K.; Grimes, C. A. High Efficiency Double Heterojunction Polymer Photovoltaic Cells Using Highly Ordered TiO_2 Nanotube Arrays. *Appl. Phys. Lett.* **2007**, *91*, 152111.
(21) Chang, C.-H.; Huang, T.-K.; Lin, Y.-T.; Lin, Y.-Y.; Chen, C.-W.; Chu, T.-H.; Su, W.-F. Improved Charge Separation and Transport Efficiency in Poly (3-hexylthiophene)-TiO_2 Nanorod Bulk Heterojunction Solar Cells. *J. Mater. Chem.* **2008**, *18*, 2201−2207.
(22) Peiro, A. M.; Ravirajan, P.; Govender, K.; Boyle, D. S.; O'Brien, P.; Bradley, D. D. C.; Nelson, J.; Durrant, J. R. Hybrid Polymer/Metal Oxide Solar Cells Based on ZnO Columnar Structures. *J. Mater. Chem.* **2006**, *16*, 2088−2096.
(23) Ravirajan, P.; Peiro, A. M.; Nazeeruddin, M. K.; Graetzel, M.; Bradley, D. D. C.; Durrant, J. R.; Nelson, J. Hybrid Polymer/Zinc Oxide Photovoltaic Devices with Vertically Oriented ZnO Nanorods and an Amphiphilic Molecular Interface Layer. *J. Phys. Chem. B* **2006**, *110*, 7635−7639.
(24) Olson, D. C.; Lee, Y. J.; White, M. S.; Kopidakis, N.; Shaheen, S. E.; Ginley, D. S.; Voigt, J. A.; Hsu, J. W. P. Effect of Polymer Processing on the Performance of Poly(3-hexylthiophene)/ZnO nanorod Photovoltaic Devices. *J. Phys. Chem. C* **2007**, *111*, 16640−16645.
(25) Takanezawa, K.; Hirota, K.; Wei, Q.-S.; Tajima, K.; Hashimoto, K. Efficient Charge Collection with ZnO Nanorod Array in Hybrid Photovoltaic Devices. *J. Phys. Chem. C* **2007**, *111*, 7218−7223.
(26) Yu, K.; Chen, J. Enhancing Solar Cell Efficiencies through 1-D Nanostructures. *Nanoscale Res. Lett.* **2009**, *4*, 1−10.
(27) Lee, T.-H.; Sue, H.-J.; Cheng, X. ZnO and Conjugated Polymer Bulk Heterojunction Solar Cells Containing ZnO Nanorod Photo Anode. *Nanotechnology* **2011**, *22*, 285401.
(28) Gonzalez-Valls, I.; Lira-Cantu, M. Vertically-Aligned Nanostructures of ZnO for Excitonic Solar Cells: a Review. *Energy Environ. Sci.* **2009**, *2*, 19−34.
(29) Huang, J.; Yin, Z.; Zheng, Q. Applications of ZnO in Organic and Hybrid Solar Cells. *Energy Environ. Sci.* **2011**, *4*, 3861−3877.
(30) Baeten, L.; Conings, B.; Boyen, H.-G.; D'Haen, J.; Hardy, A.; D'Oileslaeger, M.; Manca, J. V.; van Bael, M. K. Towards Efficient Hybrid Solar Cells Based on Fully Polymer Infiltrated ZnO Nanorod Arrays. *Adv. Mater.* **2011**, *23*, 2802−2805.
(31) Unalan, H. E.; Hiralal, P.; Kuo, D.; Parekh, B.; Amaratunga, G.; Chhowalla, M. Flexible Organic Photovoltaics from Zinc Oxide Nanowires Grown on Transparent and Conducting Single Walled Carbon Nanotube Thin Films. *J. Mater. Chem.* **2008**, *18*, 5909−5912.
(32) Tam, K.; Cheung, C.; Leung, Y.; Djurišic, A.; Ling, C.; Beling, C.; Fung, S.; Kwok, W.; Chan, W.; Phillips, D. Defects in ZnO Nanorods Prepared by a Hydrothermal Method. *J. Phys. Chem. B* **2006**, *110*, 20865−20871.
(33) Schmidt-Mende, L.; MacManus-Driscoll, J. L. ZnO-Nanostructures, Defects, and Devices. *Mater. Today* **2007**, *10*, 40−48.
(34) McCluskey, M.; Jokela, S. Defects in ZnO. *J. Appl. Phys.* **2009**, *106*, 071101−071103.
(35) Olson, D. C.; Shaheen, S. E.; White, M. S.; Mitchell, W. J.; van Hest, M. F. A. M.; Collins, R. T.; Ginley, D. S. Band-Offset Engineering for Enhanced Open-Circuit Voltage in Polymer-Oxide Hybrid Solar Cells. *Adv. Funct. Mater.* **2007**, *17*, 264−269.
(36) Steim, R.; Kogler, F. R.; Brabec, C. J. Interface Materials for Organic Solar Cells. *J. Mater. Chem.* **2010**, *20*, 2499−2512.
(37) Ratcliff, E. L.; Zacher, B.; Armstrong, N. R. Selective Interlayers and Contacts in Organic Photovoltaic Cells. *J. Phys. Chem. Lett.* **2011**, *2*, 1337−1350.
(38) Steirer, K. X.; Ndione, P. F.; Widjonarko, N. E.; Lloyd, M. T.; Meyer, J.; Ratcliff, E. L.; Kahn, A.; Armstrong, N. R.; Curtis, C. J.; Ginley, D. S.; Berry, J. J.; Olson, D. C. Enhanced Efficiency in Plastic Solar Cells via Energy Matched Solution Processed NiO_x Interlayers. *Adv. Energy Mater.* **2011**, *1*, 813−820.
(39) Ratcliff, E. L.; Garcia, A.; Paniagua, S. A.; Cowan, S. R.; Giordano, A. J.; Ginley, D. S.; Marder, S. R.; Berry, J. J.; Olson, D. C. Investigating the Influence of Interfacial Contact Properties on Open Circuit Voltages in Organic Photovoltaic Performance: Work Function Versus Selectivity. *Adv. Energy Mater.* **2013**, *3*, 647−656.
(40) van der Hofstad, T. G. J.; Nuzzo, D. D.; van Reenen, S.; Janssen, R. A.; Kemerink, M.; Meskers, S. C. J. Carrier Recombination in Polymer Fullerene Solar Cells Probed by Reversible Exchange of Charge between the Active Layer and Electrodes Induced by a Linearly Varying Voltage. *J. Phys. Chem. C* **2013**, *117*, 3210−3220.
(41) Zacher, B.; Gantz, J. L.; Richards, R. E.; Amstrong, N. R. Organic Solar Cell-at the Interface. *J. Phys. Chem. Lett.* **2013**, *4*, 1949−1952.
(42) Ravirajan, P.; Peiro, A. M.; Nazeeruddin, M. K.; Gratzel, M.; Bradley, D. D. C.; Durrant, J. R.; Nelson, J. Hybrid Polymer/Zinc Oxide Photovoltaic Devices with Vertically Oriented ZnO Nanorods and an Amphiphilic Molecular Interface Layer. *J. Phys. Chem. B* **2006**, *110*, 7635−7639.
(43) Boucle, J.; Chyla, S.; Shaffer, M. S. P.; Durrant, J. R.; Bradley, D. D. C.; Nelson, J. Hybrid Solar Cells from a Blend of Poly(3-hexylthiophene) and Ligand-Capped TiO_2 Nanorods. *Adv. Funct. Mater.* **2008**, *18*, 622−633.
(44) Krunks, M.; Katerski, A.; Dedova, T.; Acik, I. O.; Mere, A. Nanostructured Solar Cell Based on Spray Pyrolysis Deposited ZnO Nanorod Array. *Sol. Energy Mater. Sol. Cells* **2008**, *92*, 1016−1019.
(45) Zhu, R.; Jiang, C. Y.; Liu, B.; Ramakrishna, S. Highly Efficient Nanoporous TiO_2-Polythiophene Hybrid Solar Cells Based on Interfacial Modification Using a Metal-Free Organic Dye. *Adv. Mater.* **2009**, *21*, 994−1000.

(46) Lin, Y. Y.; Chu, T. H.; Li, S. S.; Chuang, C. H.; Chang, C. H.; Su, W. F.; Chang, C.-P.; Chu, M.-W.; Chen, C.-W. Interfacial Nanostructuring on the Performance of Polymer/TiO_2 Nanorod Bulk Heterojunction Solar Cells. *J. Am. Chem. Soc.* **2009**, *131*, 3644−3649.
(47) Said, A. J.; Poize, G.; Martini, C.; Ferry, D.; Marine, W.; Giorgio, S.; Fages, F.; Hocq, J.; Bouclé, J.; Nelson, J.; Durrant, J. R.; Ackermann, J. Hybrid Bulk Heterojunction Solar Cells Based on P3HT and Porphyrin-Modified ZnO Nanorods. *J. Phys. Chem. C* **2010**, *114*, 11273−11278.
(48) AbdulAlmohsin, S.; Cui, J. B. Graphene-Enriched P3HT and Porphyrin-Modified ZnO Nanowire Arrays for Hybrid Solar Cell Applications. *J. Phys. Chem. C* **2012**, *116*, 9433−9438.
(49) Chen, J.-Y.; Hsu, F.-C.; Sung, Y.-M.; Chen, Y.-F. Enhanced Charge Transport in Hybrid Polymer/ZnO-Nanorod Solar Cells Assisted by Conductive Small Molecules. *J. Mater. Chem.* **2012**, *22*, 15726−15731.
(50) Ruankham, P.; Yoshikawa, S.; Sagawa, T. Effect of the Morphology of Nanostructured ZnO and Interface Modification on the Device Configuration and Charge Transport of ZnO/Polymer Hybrid Solar Cells. *Phys. Chem. Chem. Phys.* **2013**, *15*, 9516−9522.
(51) Mor, G. K.; Kim, S.; Paulose, M.; Varghese, O. K.; Shankar, K.; Basham, J.; Grimes, C. A. Visible to Near-Infrared Light Harvesting in TiO_2 Nanotube Array−P3HT Based Heterojunction Solar Cells. *Nano Lett.* **2009**, *9*, 4250−4257.
(52) Diamant, Y.; Chappel, S.; Chen, S.; Melamed, O.; Zaban, A. Core−Shell Nanoporous Electrode for Dye Sensitized Solar Cells: the Effect of Shell Characteristics on the Electronic Properties of the Electrode. *Coord. Chem. Rev.* **2004**, *248*, 1271−1276.
(53) Zhao, J.; Wu, L.; Zhi, J. Fabrication of Micropatterned ZnO/SiO_2 Core/Shell Nanorod Arrays on a Nanocrystalline Diamond Film and Their Application to DNA Hybridization Detection. *J. Mater. Chem.* **2008**, *18*, 2459−2465.
(54) Plank, N.; Snaith, H.; Ducati, C.; Bendall, J.; Schmidt-Mende, L.; Welland, M. A Simple Low Temperature Synthesis Route for ZnO−MgO Core−Shell Nanowires. *Nanotechnology* **2008**, *19*, 465603.
(55) Greene, L. E.; Law, M.; Yuhas, B. D.; Yang, P. ZnO-TiO_2 Core-Shell Nanorod/P3HT Solar Cells. *J. Phys. Chem. C* **2007**, *111*, 18451−18456.
(56) Li, Y.; Lu, P.; Jiang, M.; Dhakal, R.; Thapaliya, P.; Peng, Z.; Jha, B.; Yan, X. Femtosecond Time-Resolved Fluorescence Study of TiO_2-Coated ZnO Nanorods/P3HT Photovoltaic Films. *J. Phys. Chem. C* **2012**, *116*, 25248−25256.
(57) Guo, D.; Wang, J.; Cui, C.; Li, P.; Zhong, X.; Wang, F.; Yuan, S.; Zhang, K.; Zhou, Y. ZnO@TiO_2 Core-Shell Nanorod Arrays with Enhanced Photoelectrochemical Performance. *Sol. Energy* **2013**, *95*, 237−245.
(58) Li, Y.; Li, S.; Jin, L.; Murowchick, J. B.; Peng, Z. Carbon Nanoparticles as an Interfacial Layer Between TiO_2-Coated ZnO Nanorod Arrays and Conjugated Polymers for High-Photocurrent Hybrid Solar Cells. *RSC Adv.* **2013**, *3*, 16308−16312.
(59) Wu, F.; Cui, Q.; Qui, Z.; Liu, C.; Zhang, H.; Shen, W.; Wang, M. Improved Open-Circuit Voltage in Polymer/Oxide-Nanoarray Hybrid Solar Cells by Formation of Homogeneous Metal Oxide Core/Shell Structures. *ACS Appl. Mater, Interfaces* **2013**, *5*, 3246−3254.
(60) Lee, J.-H.; Ko, K.-H.; Park, B.-O. Electrical and Optical Properties of ZnO Transparent Conducting Films by the Sol−gel Method. *J. Crys. Grow.* **2003**, *247*, 119−125.
(61) Dennler, G.; Scharber, M. C.; Brabec, C. J. Polymer-Fullerene Bulk-Heterojunction Solar Cells. *Adv. Mater.* **2009**, *21*, 1−16.
(62) Chang, C.-Y.; Tsai, F.-Y. Efficient and Air-Stable Plastics-Based Polymer Solar Cells Enabled by Atomic Layer Deposition. *J. Mater. Chem.* **2011**, *21*, 5710−5715.
(63) Jin, M.-J.; Jo, J.; Neupane, G. P.; Kim, J.; An, K.-S.; Yoo, J.-W. Tuning of Undoped ZnO Thin Film via Plasma Enhanced Atomic Layer Deposition and Its Application for an Inverted Polymer Solar Cell. *AIP Adv.* **2013**, *3*, 102114.
(64) Jiang, C.; Lunt, R. R.; Duxbury, P. M.; Zhang, P. P. High-Performance Inverted Solar Cells with a Controlled ZnO Buffer Layer. *RSC Adv.* **2014**, *4*, 3604−3610.
(65) von Roos, O. A Simple Theory of Back Surface Field (BSF) Solar Cells. *J. Appl. Phys.* **1978**, *49*, 3503−3511.
(66) Park, K.; Zhang, Q.; Garcia, B. B.; Zhou, X.; Jeong, Y.-H.; Cao, G. Effect of an Ultrathin TiO_2 Layer Coated on Submicrometer-Sized ZnO Nanocrystallite Aggregates by Atomic Layer Deposition on the Performance of Dye-Sensitized Solar Cells. *Adv. Mater.* **2010**, *22*, 2329−2332.
(67) Park, K.; Zhang, Q.; Garcia, B. B.; Cao, G. Effect of Annealing Temperature on TiO2-ZnO Core-Shell Aggregate Photoelectrodes of Dye-Sensitized Solar Cells. *J. Phys. Chem. C* **2011**, *115*, 4927−4934.
(68) Zhao, R.; Zhu, L.; Cai, F.; Yang, Z.; Gu, X.; Huang, J.; Cao, L. ZnO/TiO2 Core-Shell Nanowire Arrays for Enhanced Dye-Sensitized Solar Cell Efficiency. *Appl. Phys. A: Mater. Sci. Process.* **2013**, *113*, 67−73.
(69) Sah, C. T.; Noyce, R. N.; Shockley, W. Carrier Generation and Recombination in p-n Junctions and p-n Junction Characteristics. *Proc. IRE* **1957**, *45*, 1228−1243.
(70) Street, R. A.; Schoendorf, M.; Roy, A.; Lee, J. H. Interface State Recombination in Organic Solar Cells. *Phys. Rev. B* **2010**, *81*, 205307.
(71) Kirchartz, T.; Pieters, B. E.; Kirkpatrick, J.; Rau, U.; Nelson, J. Recombination via Tail States in Polythiophene: Fullerene Solar Cells. *Phys. Rev. B* **2011**, *83*, 115209.
(72) Cowan, S. R.; Leong, W. L.; Banerji, N.; Dennler, G.; Heeger, A. J. Identifying a Threshold Impurity Level for Organic Solar Cells: Enhanced First-Order Recombination Via Well-Defined PC84BM Traps in Organic Bulk Heterojunction Solar Cells. *Adv. Funct. Mater.* **2011**, *21*, 3083−3092.
(73) Ohkita, H.; Ito, S. Transient Absorption Spectroscopy of Polymer-Based Thin-Film Solar Cells. *Polymer* **2011**, *52*, 4397−4417.
(74) Clarke, T. M.; Lungenschmied, C.; Peet, J.; Drolet, N.; Sunahara, K.; Furube, A.; Mozer, A. J. Photodegradation in Encapsulated Silole-Based Polymer: PCBM Solar Cells Investigated using Transient Absorption Spectroscopy and Charge Extraction Measurements. *Adv. Energy Mater.* **2013**, *3*, 1473−1483.
(75) Grancini, G.; Polli, D.; Fazzi, D.; Cabanillas-Gonzalez, J.; Cerullo, G.; Lanzani, G. Transient Absorption Imaging of P3HT:PCBM Photovoltaic Blend: Evidence For Interfacial Charge Transfer State. *J. Phys. Chem. Lett.* **2011**, *2*, 1099−1105.
(76) Ban, T.; Hasegawa, H.; Sato, K.; Watanabe, T.; Takahashi, H. A Novel Large-Scale OXC Architecture and an Experimental System that Utilizes Wavelength Path Switching and Fiber Selection. *Opt. Express* **2013**, *21*, 469−477.
(77) Suresh, M. S. Measurement of Solar Cell Parameters Using Impedance Spectroscopy. *Sol. Energy Mater. Sol. Cells* **1996**, *43*, 21−28.
(78) van de Lagemaat, J.; Park, N.-G.; Frank, A. J. Influence of Electrical Potential Distribution, Charge Transport, and Recombination on the Photopotential and Photocurrent Conversion Efficiency of Dye-Sensitized Nanocrystalline TiO_2 Solar Cells: A Study by Electrical Impedance and Optical Modulation Techniques. *J. Phys. Chem. B* **2000**, *104*, 2044−2052.
(79) Wang, Q.; Moser, J.-E.; Crätzel, M. Electrochemical Impedance Spectroscopic Analysis of Dye-Sensitized Solar Cells. *J. Phys. Chem. B* **2005**, *109*, 14945−14953.
(80) Xu, C.; Wu, J.; Desai, U. V.; Gao, D. High-Efficiency Solid-State Dye-Sensitized Solar Cells Based on TiO_2-Coated ZnO Nanowire Arrays. *Nano Lett.* **2012**, *12*, 2420−2424.